HHS Public Access

Author manuscript

Opt Lett. Author manuscript; available in PMC 2021 July 01.

Published in final edited form as:

Opt Lett. 2020 July 01; 45(13): 3605–3608. doi:10.1364/OL.396023.

High-speed fiber-optic scanning nonlinear endomicroscopy for imaging neuron dynamics *in vivo*

Hyeon-Cheol Park[1], **Honghua Guan**[2], **Ang Li**[1], **Yuanlei Yue**[3], **Ming-Jun Li**[4], **Hui Lu**[3], **Xingde Li**[1,2,*]

[1]Department of Biomedical Engineering, Johns Hopkins University School of Medicine, Baltimore, Maryland 21205, USA

[2]Department of Electrical and Computer Engineering, Johns Hopkins University, Baltimore, Maryland 21218, USA

[3]Department of Pharmacology and Physiology, George Washington University School of Medicine, Washington, DC 20052, USA

[4]Science and Technology Division, Corning Incorporated, Corning, New York 14831, USA

Abstract

Fiber-optic-based two-photon fluorescence endomicroscopy is emerging as an enabling technology for *in vivo* histological imaging of internal organs and functional neuronal imaging on freely-behaving animals. However, high-speed imaging remains challenging due to the expense of miniaturization and lack of suited fast beam scanners. For many applications, a higher imaging speed is highly desired, especially for monitoring functional dynamics such as transient dendritic responses in neuroscience. This Letter reports the development of a fast fiber-optic scanning endomicroscope with an imaging speed higher than 26 frames/s. *In vivo* neural dynamics imaging with the high-speed endomicroscope was performed on a freely-behaving mouse over the primary motor cortex that expressed GCaMP6m. The results demonstrate its capability of real-time monitoring of transient neuronal dynamics with very fine temporal resolution.

Multi-photon fluorescence (MPF) microscopy is an advanced 3D imaging technology capable of structural, molecular, and biochemical/metabolic imaging of biological tissues in real-time at subcellular resolution [1–5]. Recent development of the miniaturized nonlinear endomicroscopy platform expands the application of MPF imaging to internal organs and enables *in vivo* label-free histological imaging [6]. Moreover, the compact footprint and light weight of the MPF endomicroscope enabled dynamic neuronal functional imaging of freely-behaving rodents with a head-mounted configuration. Among various types of MPF endomicroscopes, the one based on a resonant fiber-optic scanner has attractive advantages of a forward-looking configuration (without the need for beam folding) and thus the result compactness [7–14]. In particular, a resonant fiber-optic scanner with a tubular piezoelectric (PZT) actuator has been widely adopted for various endoscopic applications due to its

*Corresponding author: xingde@jhu.edu.

Disclosures. The authors declare no conflicts of interest.

relatively simple, compact, and cylindrical design, which is compatible with a typical medical endoscope [7–12]. However, the imaging frame rate of the previously reported fiber-optic scanning MPF endomicroscopes is limited to less than eight frames per second (fps) [9], mainly due to the unstable scanning of the fiber-optic cantilever at higher speeds. A higher imaging frame rate is crucial in many applications not only for minimizing motion artifacts, but also for monitoring functional dynamics. Particularly, there have been increasing demands on a higher imaging speed in neuroscience applications, especially for monitoring transient calcium dynamics of neurons or dendrites on freely-behaving animal models [15–18]. In this Letter, we developed a high-speed resonant fiber-optic scanning MPF endomicroscope affording an imaging frame rate over 26 fps, and demonstrated its capability of real-time neuronal activity monitoring of freely-behaving rodents.

The typical design of a resonant fiber-optic scanning endomicroscope employs a cantilevered optical fiber attached to the distal end of a tubular PZT actuator. The fiber cantilever is resonantly oscillated to amplify inherently small deflection of the PZT actuator (typically a few microns). The imaging frame rate of a resonant fiber-optic endomicroscope can be increased by increasing the resonant frequency of the cantilever which follows the inverse square of the cantilever length L_c, i.e., $f_r \propto 1/L_c^2$. Therefore, a higher imaging frame rate can be achieved by decreasing the cantilever length. However, reducing the cantilever length is at the expense of the mechanical flexibility and makes it hard to obtain a sufficient scanning amplitude. Another technical challenge for increasing the scanning speed of a resonant fiber-optic scanner is mechanical cross coupling between the two orthogonal scanning axes (x and y). Due to the circularly symmetry of a fiber cantilever, resonant frequencies along x and y directions are identical and become vulnerable to mechanical cross-coupling forces [19]. Any small amount of coupling forces could be amplified at the resonance and interfere with the other axis, which not only deteriorates scan trajectories, but also increases nonlinear behaviors of the scanner such as hysteresis. It is becoming more significant at a higher frame rate, where the scanning amplitude needs to be more rapidly modulated. Moreover, any eccentricity of a tubular PZT actuator or fiber cantilever (i.e., the eccentricity between core and claddings) due to inevitable manufacturing tolerance shifts the geometric center from the PZT force direction, which makes it even harder to avoid mechanical cross coupling. Therefore, one crucial engineering challenge to achieve a high scanning speed is effective transfer of the vibrational forces generated by the PZT actuator to the fiber cantilever so that a sufficient cantilever scanning amplitude can be reached at the fiber tip. Another challenge is precision alignment of all the mechanical components in order to minimize mechanical cross coupling.

Figure 1A shows the schematic of a resonant fiber-optic scanning endomicroscope assembly. The double-clad fiber (DCF) cantilever needs to be well aligned with both the optical and mechanical axes of the endomicroscope to achieve optimal optical and mechanical performance. A slight dislocation of the DCF cantilever off the center would induce mechanical cross coupling or force imbalance between the two orthogonal scanning axes. The misalignment can also degrade the optical performance such as vignetting at the edge of the field of view (FOV) or off-axis aberrations. For the same reasons, the PZT actuator also needs to be precisely placed along the center axis of the endomicroscope. The precise concentric alignment of each component was secured by using a reference metal rod (which

has an identical diameter as the DCF, 250 μm) and a precision-machined base. The base consists of an opening at the center with a diameter slightly larger than the DCF. The metal rod was first inserted through the opening, as a global reference of a central axis during the entire assembling process, and replaced with a DCF during the last step. An 8 mm long PZT actuator (PZT-5H) was then carefully aligned along the central axis with the guidance of the reference rod before being glued to the base. In order to effectively transfer the vibrational forces, a custom adapter made of 304 stainless steel was used between the PZT actuator and the fiber cantilever. The adapter was installed following the reference rod and glued to the distal end of the PZT actuator. At the final step, an ~7 mm long custom DCF (Corning Inc., NA–0.12 for the core and NA–0.35 for the inner cladding) was cantilevered and glued to the adapter after replacing the reference metal rod. It is noted that all the components were made with hard materials (including the glue of >5000 psi strength) in order to minimize damping loss and preserve the vibrational forces at the joints.

The distal end of the endomicroscope, including a superachromatic micro-objective lens (GRINTECH GmbH, NA–0.18 on the fiber side and NA–0.75 on the tissue side) of a 2.25 mm diameter, was fully encased inside a hypodermic metal tube of a 2.8 mm outer diameter. The micro-objective lens provides a 300 μm working distance (in air) with a ~5× magnification. In order to make the micro-objective concentric with the longitudinal axis of the scanner, a precision-made snug-fit adapter was used between the micro-objective and the housing metal tube. The distance between the DCF tip and the micro-objective surface is crucial for controlling and optimizing the optical performance parameters of the endomicroscope, including working distance and excitation/collection efficiencies. This distance was fine-tuned by using a low-coherence interferometer during endomicroscope assembling. A femtosecond laser centered at 800 nm with an ~50 nm 3 dB spectral bandwidth and a corresponding ~5.6 μm coherence length, was coupled into a core of the DCF. The distance between the DCF tip and the micro-objective was measured and adjusted to 200 μm by monitoring the interference signal from the back-reflected lights from the flat-cleaved DCF tip and the first surface of the micro-objective. The PZT drive wires and the DCF were further protected with a torque coil, and the proximal end of the DCF was connectorized with an FC/APC connector for a plug-and-play operation. Figures 1B and 1D show a photograph of a fully assembled endomicroscope. The overall rigid length of the endomicroscope was 24 mm. The precision modular components employed in the endomicroscope ensure accurate alignment during the assembling process and, as shown in Fig. 1C (front view image of the endomicroscope), the DCF cantilever was well aligned with the center of the endomicroscope.

The beam scanning performance of the endomicroscope was investigated. Figure 2A shows the resonant frequency response of the fiber cantilever. A ~7 mm long DCF cantilever produces resonant frequencies of 3350 and 3410 Hz for the x and y axes, respectively. The resonant frequency mismatch between the two orthogonal axes was less than 2%, which indicates that the mechanical symmetricities were well managed, despite intrinsic manufacturing tolerances of the components. As a result, the coupling forces were minimized, and nice line scan patterns for both axes were achieved, as shown in the inset images of Fig. 2A. 2D spiral scanning parameters were carefully adjusted in order to achieve a maximal FOV while minimizing the nonlinear effects. A frequency in the middle of the

two resonant frequencies, i.e., 3380 Hz, was chosen as the PZT actuation frequency for both axes. The phase difference between the drive waveforms for the two axes was adjusted until a circular beam scanning trajectory was achieved. The phase difference was set to be 165 deg. Figure 2B shows the scanning range (diameter of the FOV) of the endomicroscope with respect to the peak-to-peak drive voltage. We found that our current precision design and the use of hard materials in the scanner assembly ensure effective transfer of the vibrational forces from a PZT actuator to the DCF cantilever, and a ~150 μm of FOV (optimal FOV of the micro-objective) could be obtained with a 100 V_{AC} peak-to-peak drive voltage.

The endomicroscope was integrated with a home-built MPF imaging system. Figure 3A shows the schematic of the imaging system with the new scanning endomicroscope. A femtosecond excitation beam at 920 nm from a Ti:sapphire laser was first pre-chirped by a pair of customized grating-prisms (GRISM) to compensate for the material dispersions [20], and then coupled into the single-mode core of the DCF of the endomicroscope. The pulse width and the averaged output power at the sample were measured to ~42 fs and ~30 mW. The fluorescence photons collected by the micro-objective lens were transmitted through the DCF core and inner cladding and directed to a photomultiplier tube (PMT) at the proximal end of the probe, and the signal was digitized with a DAQ card at 5 MHz (0.2 μs pixel dwell time). The lateral and axial resolutions of the endomicroscope were measured to be 0.8 and 6.1 μm, respectively.

In vivo high-speed imaging of neuronal dynamics with the new endomicroscope was demonstrated by recording neuronal activities of a freely-behaving mouse. Figure 3B shows the photograph of the imaging setup with the endomicroscope mounted on the head of a freely-behaving mouse. A craniotomy of an ~4 mm diameter opening was previously performed over the primary motor cortex of a mixed C79/219 rodent under anesthesia. A 100 μm thick cover glass was used to cover the cortex and glued to the skull with dental cement to form a cranial window for imaging. Neurons on the motor cortex expressed GCaMP6m via viral infection, and neuronal activities were accessed by imaging GCaMP6m fluorescence. The endomicroscope was mounted over the cranial window with a custom holder. All the animal housing and experimentation procedures were performed under protocols approved by the institutional animal care and use committees of the Johns Hopkins University and the George Washington University.

Figures 4A and 4B show representative MPF images of neuronal activities of a freely-behaving mouse captured over a similar FOV with the endomicroscope at two frame rates: 3.3 fps (Visualization 1) with 1490 × 1024 pixels (circumferential x radial) and 26.4 fps (Visualization 2) with 1490 × 128 pixels. At a 26.4 fps, we slightly compromised the image resolution along the radial direction. The final image of 512 × 512 pixels was reconstructed by digital interpolation along the radial direction and down-sampling along the circumferential direction. The somatic calcium dynamics were reflected in the normalized GCaMP6 fluorescence signals ($\Delta F/F$). Figures 4C and 4D shows calcium dynamics of a given neuron (indicated with the dotted circle in Figs. 4A and 4B) recorded over 5 min at each frame rate. At a 26.4 fps, we were able to record functional dynamics with much finer temporal resolution. Zoomed-in views of a portion of the curves in Figs. 4C and 4D show four representative neuronal responses. Some immediate signal changes or minor peaks

(indicated with red arrows), particularly those associated with consecutive responses within a short period of time, can be readily identified at a higher imaging speed. In contrast, transient responses can be easily overlooked at a lower imaging speed due to averaging with neighboring signals.

Dendritic activities of the freely-behaving mouse were also recorded with the endomicroscope. Figure 5A shows calcium dynamics of a dendrite captured at 26.4 fps (indicated with a white arrow in Figs. 5B–5K). The normalized GCaMP6 fluorescence signals were integrated along the dendrite. Dendritic dynamic signals are often much shorter than somatic signals. Figures 5B–5K show time-series snapshots of dendritic calcium dynamics near a signal peak, captured at 3.3 fps (B-E, Visualization 3), and 26.4 fps (F-K, Visualization 4). At 3.3 fps, fluorescence signals from dendrites could be seen in a given frame image, but quickly dimmed in consecutive images. However, at the higher rate (26.4 fps), we were able to capture much more details of the transient dendritic activities. For example, we could observe the propagation of the dendrite fluorescence signal from top right of the FOV to the bottom left (as indicated with dashed arrows in Fig. 5I) with a speed of ~100 μm⁄s, which was on the same order of calcium wave propagation [21].

To conclude, we developed a high-speed resonant fiber-optic scanning MPF endomicroscope. Robust and precise engineering and assembly procedures secure effective actuation force transfer, as well as scanning stability at a higher scanning speed, resulting in ~10-fold increase of an imaging speed compared to our previous design [10]. Performance of the high-speed (video-rate) endomicroscope was demonstrated by *in vivo* neuronal dynamics imaging on a freely-behaving mouse. The results show the capability of the high-speed endomicroscope for monitoring transient neuronal dynamics with much finer temporal resolution, and potential as a useful tool for fundamental neuroscience research. The current endomicroscope employs a relatively larger objective lens of a 2.25 mm diameter to obtain a long working distance for imaging neurons through the cranial window, and the resulting overall outer diameter of the endomicroscope was 2.8 mm (cf. OD_{PZT}~ 1.5 mm). Further probe miniaturization down to ~2 mm in diameter is possible by using a smaller objective lens. It is recognized that, with further miniaturization, the high-speed endomicroscope can also be applied to internal organs for *in vivo* label-free histological imaging or functional imaging, and can potentially play a role in a wide range of translational applications.

Acknowledgments

Funding. National Institutes of Health (R01CA247595); Medical Technology Enterprise Consortium (MTEC-16-02-BMI-09).

REFERENCES

1. Denk W, Strickler JH, and Webb WW, Science 248, 73 (1990). [PubMed: 2321027]
2. Xu C, Zipfel W, Shear JB, Williams RM, and Webb WW, Proc. Natl. Acad. Sci. USA 93, 10763 (1996). [PubMed: 8855254]
3. Zipfel WR, Williams RM, and Webb WW, Nat. Biotechnol 21, 1369 (2003). [PubMed: 14595365]
4. Helmchen F and Denk W, Nat. Methods 2, 932 (2005). [PubMed: 16299478]
5. Svoboda K and Yasuda R, Neuron 50, 823 (2006). [PubMed: 16772166]

6. Flusberg BA, Cocker ED, Piyawattanametha W, Jung JC, Cheung ELM, and Schnitzer MJ, Nat. Methods 2, 941 (2005). [PubMed: 16299479]
7. Myaing MT, MacDonald DJ, and Li XD, Opt. Lett 31, 1076 (2006). [PubMed: 16625908]
8. Zhang Y, Akins ML, Murari K, Xi J, Li M-J, Luby-Phelps K, Mahendroo M, and Li XD, Proc. Natl. Acad. Sci. USA 109, 12878 (2012). [PubMed: 22826263]
9. Ducourthial G, Leclerc P, Mansuryan T, Fabert M, Brevier J, Habert R, Braud F, Batrin R, Vever-Bizet C, Bourg-Heckly G, Thiberville L, Druilhe A, Kudlinski A, and Louradour F, Sci. Rep 5, 18303 (2015). [PubMed: 26673905]
10. Liang W, Hall G, Messerschmidt B, Li M-J, and Li XD, Light Sci. Appl 6, e17082 (2017). [PubMed: 29854567]
11. Akhoundi F, Qin Y, Peyghambarian N, Barton JK, and Kieu K, Biomed. Opt. Express 9, 2326 (2018). [PubMed: 29760991]
12. Kim DY, Hwang K, Ahn J, Seo Y-H, Kim J-B, Lee S, Yoon J-H, Kong E, Jeong Y, Jon S, Kim P, and Jeong K-H, Sci. Rep. 9, 3560 (2019). [PubMed: 30837501]
13. Rivera DR, Brown CM, Ouzounov DG, Pavlova I, Kobat D, Webb WW, and Xu C, Proc. Natl. Acad. Sci. USA 108, 17598 (2011). [PubMed: 22006303]
14. Park H-C, Zhang X, Yuan W, Zhou L, Xie H, and Li XD, Opt. Lett 44, 2232 (2019). [PubMed: 31042191]
15. Helmchen F, Fee MS, Tank DW, and Denk W, Neuron 31, 903 (2001). [PubMed: 11580892]
16. Engelbrecht CJ, Johnston RS, Seibel EJ, and Helmchen F, Opt. Express 16, 5556 (2008). [PubMed: 18542658]
17. Zong W, Wu R, Li M, Hu Y, Li Y, Li J, Rong H, Wu H, Xu Y, Lu Y, Jia H, Fan M, Zhou Z, Zhang Y, Wang A, Chen L, and Cheng H, Nat. Methods 14, 713 (2017). [PubMed: 28553965]
18. Ozbay BN, Futia GL, Ma M, Bright VM, Gopinath JT, Hughes EG, Restrepo D, and Gibson EA, Sci. Rep 8, 8108 (2018). [PubMed: 29802371]
19. Park H-C, Seo Y-H, Hwang K, Lim J-K, Yoon SZ, and Jeong K-H, Opt. Lett 39, 6675 (2014). [PubMed: 25490650]
20. Kalashyan M, Lefort C, Martínez-León L, Mansuryan T, Mouradian L, and Louradour F, Opt. Express 20, 25624 (2012). [PubMed: 23187381]
21. Ross W, Nat. Rev. Neurosci 13, 157 (2012). [PubMed: 22314443]

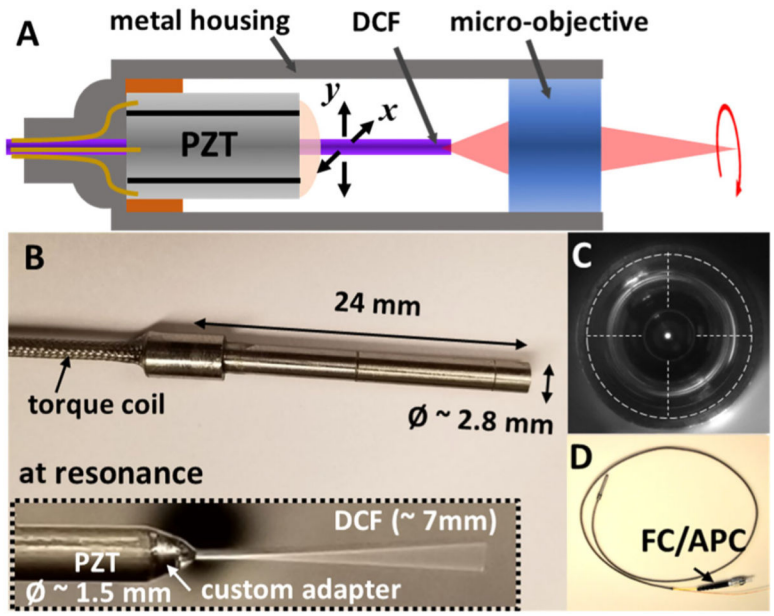

Fig. 1.

A, a schematic of a resonant fiber-optic scanning endomicroscope. A precision-machined PZT base and a custom adapter were used for centering each component and ensuring effective force transfer from the PZT actuator to the fiber cantilever. B, photograph of a fully assembled endomicroscope. The fiber scanner and a superachromatic micro-objective are encased inside a hypodermic metal tube of a 2.8 mm diameter and a 24 mm overall rigid length. A ~7 mm long DCF was cantilevered at the distal end of a PZT actuator and resonantly scanned (inset). C, front view of an endomicroscope showing the DCF was concentrically aligned with the longitudinal axis of the endomicroscope. D, photograph of an assembled endomicroscope with a protective torque coil over the fiber and PZT drive wires and an FC/APC connector at its proximal end.

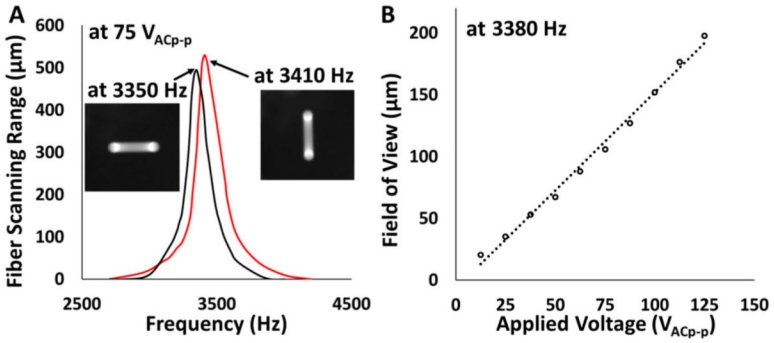

Fig. 2.

A, frequency responses of the resonant fiber-optic scanner, measured at a 75 V_{AC} peak-to-peak drive voltage. The resonant frequencies were 3350 and 3410 Hz for the *x* and *y* scanning axis, respectively. The inset images show line scan patterns at each resonance. Precision assembling ensures mechanical symmetry of the PZT actuator and the fiber cantilever and minimizes the coupling forces. B, diameter of the endomicroscope imaging FOV with respect to the PZT drive voltages. An FOV greater than 150 μm in diameter can be achievedwitha100 V_{AC} peak-to-peak drive voltage.

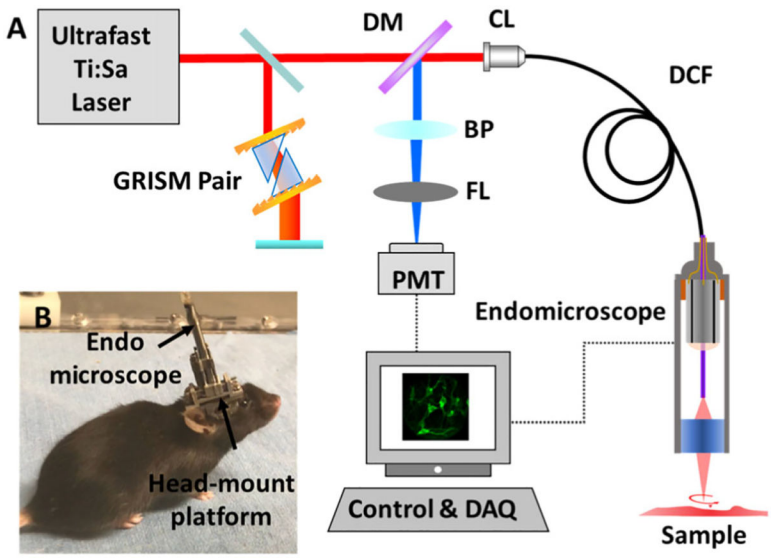

Fig. 3.

A, schematic of the MPF endomicroscopy system. B, photograph of a brain imaging setup for a freely-behaving mouse. The endomicroscope was mounted on top of a cranial window over the mouse cortex. DM, dichroic mirror; BP, bandpass filter; FL, focusing lens; PMT, photomultiplier tube; CL, coupling lens.

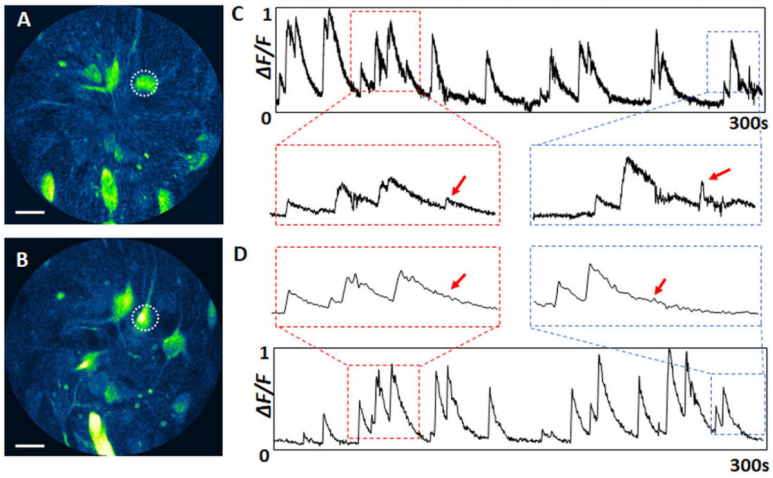

Fig.4.

A and B, representative MPF images of neuronal activities in the primary motor cortex of a freely-behaving rodent captured with the endomicroscope at imaging speeds of A, 26.4 fps and B, 3.3 fps. C and D, recorded calcium dynamics of a neuron indicated with a dotted circle in A and B over 5 min: Cat 26.4 fps, Dat 3.3 fps. Scale bars: 20 μm.

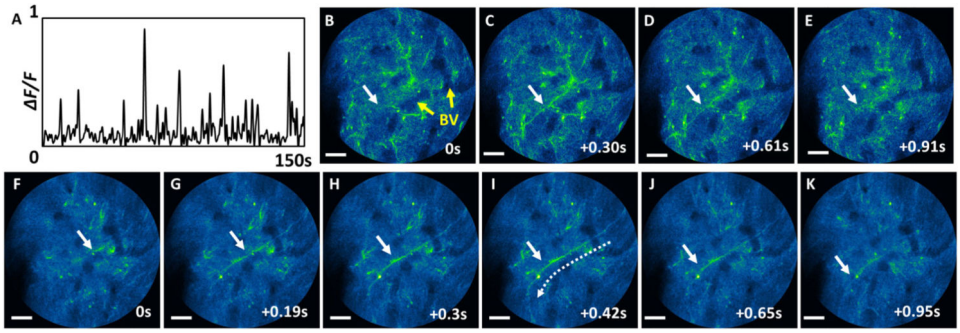

Fig. 5.

Dendritic activities of a freely-behaving mouse captured with the endomicroscope. A, calcium dynamics of a dendrite indicated with a white arrow captured at 26.4 fps. B–K, time-series images of a dendrite burst captured at B–E, 3.3 fps and F–K, 26.4 fps. The blood vessels are indicated with yellow arrows in B, and similar blood vessels can be seen in all the other images. Scale bars: 20 μm.